Primary Processes and Structure of the Photosystem II Reaction Center. 5. Modeling of the Fluorescence Kinetics of the D_1-D_2-cyt-b_{559} Complex at 77 K†

Lars Konermann, Guido Gatzen, and Alfred R. Holzwarth*

Max-Planck-Institut für Strahlenchemie, Stiftstrasse 34-36, D-45470 Mülheim a.d. Ruhr, Germany

Received: March 5, 1996; In Final Form: January 17, 1997⊗

The fluorescence kinetics of the photosystem II reaction center (D_1-D_2-cyt-b_{559} complex, PSII-RC) at a temperature of 77 K has been analyzed. A kinetic model is presented that takes into account the inhomogeneous broadening of the pigment spectra and the heterogeneity in the pigment composition of the sample. This work is based on the spectral analysis that was presented in a recent study to describe the absorption properties of the PSII-RC (Konermann, L.; Holzwarth, A. R. *Biochemistry* **1996**, *35*, 829). For the kinetic model, the Förster theory was applied to calculate the rate constants for pairwise energy transfer. Due to the inhomogeneous broadening of the spectra the energy transfer rates show a pronounced dispersion which has severe consequences for the excited state kinetics. We tested different models for radical pair formation and recombination to describe the data. Only with a model that includes several sequential radical pairs we could obtain acceptable agreement with the experimental fluorescence kinetics. A model with a static Gaussian distribution for the free energy difference of charge separation did not fit the data. The occurrence of sequential radical pair states is interpreted as a dynamic relaxation process of the protein surrounding triggered by the sudden creation of a pair of ions. The temperature dependence of the stationary fluorescence quantum yield and the temperature dependence of the stationary spectrum, as well as other experimental data predicted by the kinetic model, is in good agreement with experimental results.

Introduction

Since the first isolation of the reaction center (RC) of photosystem II (D_1-D_2-cyt-b_{559} complex, PSII-RC),[1] a variety of studies has been carried out to elucidate the structure and function of this pigment−protein complex (for reviews, for example, see refs 2−5). Unlike the RC of purple bacteria, for which the X-ray structure has been solved at atomic resolution,[6] the structure of the PSII-RC is not yet known. However, since the amino acid sequence of the L and M proteins of the bacterial RC is highly homologous to that of the D_1 and D_2 subunits of the PSII-RC, the bacterial complex can be considered as a suitable model for the PSII-RC.[7] Nevertheless, there are some important differences between the two types of RCs: The bacterial RC binds four bacteriochlorophylls (BChls), two bacteriopheophytins (BPheos), one carotene, the quinone-type electron acceptors Q_A and Q_B, and a non-heme iron. For the PSII-RC, a pigment content of ≥ six chlorophylls[a] (Chls), two pheophytins[a] (Pheos), and two β-carotenes has been established, while both quinones and the non-heme iron are lost during the isolation procedure.[1,8,9] Another point that differs profoundly between both types of RCs concerns the shape of the $Q_y(S_0-S_1)$ region of the absorption spectrum. The pigments in the bacterial RC can be assigned approximately to specific well-resolved spectral positions, whereas the situation is much more complicated for the highly congested absorption spectrum of the PSII-RC.[10−13] This poses a considerable problem for all spectroscopic studies and especially for time-resolved measurements. The fluorescence and transient absorption kinetics are highly multiexponential and show a pronounced dependence on the excitation and detection wavelength.[14−18] In addition to the spectral congestion, the interpretation of these time-resolved data is furthermore complicated by the presence of two "antenna" Chls in the PSII-RC which have no counterparts in the bacterial RC. For this reason, the assignment of the observed lifetimes to the underlying photophysical processes is still a matter of vivid debate (for example, see refs 17−21).

Another unsolved problem is the kinetics of radical pair (RP) formation and relaxation in photosynthetic RCs. In order to explain the complex multiexponential kinetics of bacterial RCs, it has been suggested that the free energy difference for RP formation should have a static distribution giving rise to a dispersive kinetics.[22,23] On the basis of temperature dependent measurements of the triplet- and fluorescence quantum yields, a similar model was suggested for the PSII-RC.[24] An alternative explanation for the multiexponential kinetics is a radical pair relaxation coupled to motions of the protein matrix.[18,25−27] One of the aims of this study is to test whether the picture of such a static distribution in free energy differences or alternatively a dynamic radical pair relaxation model are compatible with time-resolved fluorescence data at low temperatures.

In a previous paper,[28] we presented a detailed spectral analysis in order to describe the inhomogeneously broadened absorption spectrum of the PSII-RC. This spectral model was developed with the intention to be compatible with a large variety of available experimental data. It is based on the theoretical calculation of temperature dependent line shapes for the individual pigment spectra, taking into account electron−phonon coupling[29,30] and inhomogeneous broadening.[13,31] Two of the important features of this model are that it successfully describes the pronounced temperature dependence of the PSII-RC absorption spectra and also the relationship between varying pigment stoichiometry and the shape of the spectra. In this way we obtained a decomposition for the congested absorption spectrum

* Author to whom correspondence should be addressed: E-mail, Holzwarth@mpi-muelheim.mpg.de; FAX, (+49) 208 306 3951.

† A preliminary account of this work has been presented at the 10th International Congress on Photosynthesis, Montpellier, 1995. This work is part of the Ph.D. thesis of Lars Konermann at the Heinrich-Heine-Universität, Düsseldorf. Part IV: Müller, M. G.; Hucke, M.; Reus, M.; Holzwarth, A. R. *J. Phys. Chem.* **1996**, *100*, 9527−9536.

⊗ Abstract published in *Advance ACS Abstracts,* March 1, 1997.

S1089-5647(96)00667-0 CCC: $14.00

of the PSII-RC that, for the first time, uses realistic line shapes for the individual pigments. This spectral model now forms the basis of the present work.

We shall briefly recall here the basic features of the organisation of the PSII-RC which we suggested in the framework of that spectral model.[28]: The primary electron donor P_{680} consists of a pair of excitonically coupled Chls. Together with two Pheos ($Pheo_1$ and $Pheo_2$) and two *accessory Chls* (Chl_{acc1} and Chl_{acc2}), P_{680} forms a *RC core* with a structure that resembles the organization of the purple bacterial RC. On its periphery the PSII-RC core binds two *antenna Chls* (Chl_{ant1} and Chl_{ant2}) that have no equivalents in bacterial RCs. Further on, *additional Chls* may be bound to a small fraction of the PSII-RCs in a sample. The latter can be grouped into three spectrally different pools labeled Chl_{add1}, Chl_{add2}, and Chl_{add3} which are largely responsible for the variable pigment content of the PSII-RC preparations. This model is consistent with hole-burning data,[31−34] site-electron fluorescence experiments,[13,35] and polarized singlet minus triplet spectroscopy[36] as well as with predictions from the computer-modeling studies on the structure of the PSII-RC.[37]

We pointed out that this spectral model needed to be tested further experimentally. As one of these experimental tests we apply the model in this study to the analysis of time-resolved fluorescence data at low temperature (77 K). As a consequence of the inhomogeneous broadening, the energy transfer rates in the ensemble are widely distributed which leads to a highly complex energy transfer kinetics that cannot be described in a simple rate equation model. Furthermore, in order to describe the experimental fluorescence kinetics, we will also test different models for the RP formation and recombination.

Materials and Methods

Experimental. *Samples.* The PSII-RC samples for this study were prepared from spinach leaves according to the method of van Leeuven et al.[38] Directly after the preparation, the samples were shock-frozen and stored at liquid nitrogen temperature until use. The Chl/2 Pheo ratio of the samples was measured by HPLC as described,[28] resulting in a pigment ratio of 6.3 ± 0.2 Chl/2 Pheo. The low-temperature absorption spectrum of such a sample is given in Figure 2 (corresponding to spectrum no. 5) of our previous paper.[28]

Time-Resolved Fluorescence Measurements. Fluorescence decay curves were measured by single-photon counting as described previously.[14,17] The RC samples were mixed with 60% v/v glycerol and were shock-frozen in a 0.1 mm cuvette by dipping into liquid nitrogen. It was subsequently placed in a liquid nitrogen cooled cryostat. Excitation was at 650 nm with a repetition rate of 800 KHz. The fwhm of the system response function was about 30 ps. The excitation intensity was low enough to produce less than 10% of a steady state concentration of triplets. Decays were recorded for several emission wavelengths at a resolution of both 2 and 40 ps/channel, resulting in total time windows of 3 and 120 ns, respectively. In a first step the data were analyzed globally as a sum of exponentials. The quality of the resulting fits was judged by visual inspection of the residuals and the global χ^2 value. The number of exponentials was chosen such that a good global description of the entire data/time/wavelength surface resulted. Note that the lifetimes and their corresponding decay-associated spectra (DAS) resulting from this analysis are not given any physical interpretation in this work. Rather those parameters here merely serve as an adequate mathematical description of the fluorescence time course at the various emission wavelengths. It is this time course, and not the specific set of lifetimes, that needs to be well reproduced by the kinetic model.

Kinetic Modeling. *Solving the Master Equation*. In this section we briefly describe the basic equations that describe the excited state kinetics in a sample of (homogeneous) RCs due to energy transfer and charge separation. In the next section we then introduce the necessary modifications in order to include inhomogeneous broadening and sample heterogeneity.

Let **x** be the vector of occupation probabilities (populations) for the $N-1$ excited pigments in the RC. The differential equations, which describe the kinetics in such a particle are given in eqs 1−3.[39,40] In the simplest version of the kinetic model we assume that one single RP (assigned to x_N, see eq 2) is formed in a one-step reaction from the excited primary electron donor (assigned to x_1, see eq 1). The primary electron donor can be excited either directly or via energy transfer from another pigment in the complex (assigned to x_i for $i \neq 1$ and $i \neq N$).

$$\frac{\mathrm{d}x_1}{\mathrm{d}t} = -\left(k_{CS} + \frac{1}{\tau_1} + \sum_{j=2}^{N-1} W_{j\leftarrow 1}\right)x_1 + \sum_{j=2}^{N-1} W_{1\leftarrow j}\, x_j + k_{\mathrm{REC}}\, x_N \tag{1}$$

$$\frac{\mathrm{d}x_N}{\mathrm{d}t} = k_{CS}\, x_1 - \left(k_{REC} + \frac{1}{\tau_N}\right)x_N \tag{2}$$

$$\frac{\mathrm{d}x_i}{\mathrm{d}t} = -\left(\frac{1}{\tau_i} + \sum_{j=1,j\neq i}^{N-1} W_{j\leftarrow i}\right)x_i + \sum_{j=1,j\neq i}^{N-1} W_{i\leftarrow j}\, x_j \tag{3}$$

In these equations k_{CS} denotes the charge separation rate, k_{REC} the rate constant of the RP recombination back to the excited electron donor, τ_i the intrinsic fluorescence lifetimes of the hypothetically isolated pigments, and $1/\tau_N$ the overall rate constant for the decay of the RP to the triplet and/or ground state. The initial conditions for this set of coupled differential equations for time $t = 0$ are given by the absorption spectra of the species 1 to $N-1$ at the excitation wavelength. Summarizing these differential equations the "master equation" of the system can be written as follows:

$$\frac{\mathrm{d}\mathbf{x}}{\mathrm{d}t} = \langle \mathrm{A} \rangle \cdot \mathbf{x} \tag{4}$$

Here $\langle \mathbf{A} \rangle$ denotes the transfer matrix for the RC which contains the energy and electron transfer rates. The rate constant $W_{i\leftarrow j}$ for energy transfer between a donor pigment j and an acceptor pigment i is calculated according to the Förster formula.[41,42]

$$W_{i\leftarrow j} = \frac{9000(\ln 10)}{128\pi^5 n^4 N \tau_{0j}} \frac{k_{ij}^2}{R_{ij}^6} \int_0^\infty f_j(\omega)\epsilon_i(\omega)\frac{\mathrm{d}\omega}{\omega^4} \tag{5}$$

In this formula ω denotes the wavenumber [cm^{-1}], $f_j(\omega)$ is the fluorescence spectrum of the donor pigment which is area normalized to unity, and $\epsilon_i(\omega)$ is the molar decadic extinction coefficient of the acceptor molecule. N is the Avogadro number, n the refractive index of the surrounding medium, and $\tau_{0\mathrm{j}}$ the radiative lifetime [ns] of the donor. The energy transfer rate depends upon the distance R_{ij} between the pigments and upon the orientation factor k_{ij}:

$$k_{ij} = (\boldsymbol{e}_i \mathrm{e}_\mathrm{j}) - 3(\boldsymbol{e}_i \mathrm{r}_\mathrm{ij})(\boldsymbol{e}_j \mathrm{r}_\mathrm{ij}) \tag{6}$$

where $\mathbf{e}_i$ and $\mathbf{e}_j$ are unit vectors in the direction of the Q_y transition-dipole moments and $\boldsymbol{r}_{ij}$ is the unit vector in the direction of the axis connecting the two molecules. The Förster formula is only valid in the weak coupling limit, and this requirement might not be fulfilled between all the pigments in a RC complex. Nevertheless, for our modeling we will use this formula and any limitations will be discussed later (for the

applicability of the Förster formula in case of stronger coupling see also the work of Knox and Gülen[43]). Equation 5 is used for calculating the rate constant in the case of an energetic downhill reaction, e.g., if the donor molecule has its zero phonon line (ZPL) at higher energy than the acceptor molecule. The rate constant for the corresponding uphill reaction is calculated from the downhill rate and the energy difference ΔE between the ZPL of the donor j and the acceptor molecule i according to the Boltzmann formula:[2,24,44,45]

$$W_{j\leftarrow i} = W_{i\leftarrow j} \exp(-\Delta E/k_B T) \tag{7}$$

Here k_B is the Boltzmann constant and T the absolute temperature. Equation 7 is used for two reasons: First, it ensures detailed energetic balance, and second, it provides a much better value for the uphill rate constant in case that the shape of the donor and acceptor spectra are not known exactly in the region of small overlap. However, it should be noted that in the case of properly calculated homogeneous pigment spectra, as in this work,[28] the directly calculated $W_{j\leftarrow i}$ are in perfect agreement with the ones calculated according to eq 7. The Boltzmann formula is also applied to calculate the charge recombination rate constant k_{REC} from the charge separation rate k_{CS} and the free energy difference for RP formation ΔG_{CS}.

The extension of the equations given above to a model that includes a series of sequential RP states is straightforward. In that case the primary radical pair RP_1 is formed from the excited primary electron donor in photosystem II P_{680}* in a one-step reaction just like described above. This RP_1 then relaxes by running through a series of consecutive RP states (RP_2, RP_3, RP_4, ...). Such a model contains additional parameters, for example, the rate constants for the reactions $RP_i \rightarrow RP_{i+1}$, the corresponding free energy differences between the RP states which are used to calculate the backward rate constant using eq 7, and the rate constants $1/\tau_{RP_i}$ for the overall decay of the RPs to the triplet and/or ground state. All the rate constants for the formation and decay of the RP states can be included in the transfer matrix $\langle \mathbf{A} \rangle$ (see eq 4) where each additional RP state in the model increases the dimension N. In order to fit the model kinetics to experimental time-resolved fluorescence data, eq 4 has to be solved. In this way, N lifetimes τ_k are obtained together with their corresponding amplitudes in the form of decay-associated spectra (DAS).[39,46,47] The calculated fluorescence decay curves $f(\lambda_{exc},\lambda_{em},t)$ are then given as a sum of exponentials:

$$f(\lambda_{exc},\lambda_{em},t) = \sum_{k=1}^{N} \mathrm{DAS}_k(\lambda_{exc},\lambda_{em}) \exp(-t/\tau_k) \tag{8}$$

In this equation, λ_{exc} are the excitation and emission wavelengths, respectively, and t denotes the time.

Extension to Inhomogeneous Broadening and Sample Heterogeneity. If inhomogeneous broadening and heterogeneity in the pigment content of the RCs in the sample have to be taken into account, the fluorescence decay curves can no longer be calculated according to eq 8. Inhomogeneous broadening means that the pigments in every single RC particle have their own specific absorption and emission properties due to differences in the chromophore surroundings. The ZPL positions of the homogeneous spectra are distributed according to the corresponding inhomogeneous distribution function (IDF) which is assumed to be of Gaussian shape.[48] In our model, we assumed that the energies of the single pigment spectra are uncorrelated.[31] The inhomogeneously broadened spectrum can be calculated as the convolution of the homogeneous spectrum $B(\omega)$ with its distribution function IDF(ω).

$$I(\omega) = \int_{-\infty}^{\infty} IDF(\omega_0) B(\omega-\omega_0)\, \mathrm{d}\omega_0 \tag{9}$$

From the Förster formula (eq 5) it immediately follows that, in the case of such an energetic disorder, also the energy transfer rates are not the same among corresponding pigments in different RCs, but are dispersed due to the variable overlap of the absorption and emission bands. To describe the energy transfer on a molecular level, the homogeneous absorption and emission spectra for individual chromophores have to be used in eq 5 which can be calculated from the theory of electron−phonon coupling as described in the literature.[28−30] The homogeneous fluorescence spectrum of a pigment is taken as the minor image of the absorption spectrum with respect to the ZPL. In order to describe the kinetics of a macroscopic sample with inhomogeneously broadened spectra, in principle eq 4 has to be solved for all possible combinations of homogeneous spectra, each one giving a contribution to the observed fluorescence kinetics according to eq 8. To describe the experimentally observed fluorescence kinetics, these contributions have to be integrated over the whole parameter space defined by the IDFs of the chromophores. A similar situation arises if the sample is heterogeneous in the pigment composition. This problem can be solved by summing up the fluorescence kinetics for all the different particles in the sample, weighted properly according to their respective contributions. Thus, as a result of inhomogeneous broadening and sample heterogeneity, eq 8 has to be generalized. The fluorescence decay curves (now denoted as $F(\lambda_{exc},\lambda_{em},t)$) have to be expressed in terms of a lifetime distribution $a(\lambda_{exc},\lambda_{em},\tau)$, rather than as a sum of discrete exponentials:

$$F(\lambda_{exc},\lambda_{em},t) = \int_0^{\infty} a(\lambda_{exc},\lambda_{em},\tau) \exp(-t/\tau)\, \mathrm{d}\tau \tag{10}$$

Due to the limited time resolution in our fluorescence measurements, lifetimes shorter than 1 ps were not considered for the calculation of the simulated $F(\lambda_{exc},\lambda_{cm},t)$. From eq 10 the stationary fluorescence spectrum $F_{stat}(\lambda_{exc},\lambda_{em})$ can be calculated by integration:

$$F_{stat}(\lambda_{exc},\lambda_{em}) = \int_0^{\infty} a(\lambda_{exc},\lambda_{em},\tau)\tau\, \mathrm{d}\tau \tag{11}$$

Modeling the Time-Resolved Fluorescence of the PSII-RC. In this section we will describe how the spectral model[28] can be applied properly in order to describe the fluorescence kinetics of the PSII-RC. In the case of a complex energy transfer system between several inhomogeneously broadened pigments, no analytical formula is available to solve the kinetics. Thus eq 4 has to be solved for many different (typically several hundred) spectral "arrangements".

Each arrangement represents the spectral properties and the pigment stoichiometry of a particular PSII-RC in the sample. To account for the inhomogeneous broadening in the ensemble, the ZPL positions for each pigment are chosen at random from the corresponding IDFs. This results in a specific set of energy transfer rate constants for the kinetic matrix $\langle \mathbf{A} \rangle$. Moreover, the pigment content per RC is not the same for each arrangement. We made the approximation that both Chl_{ant} are present in every RC particle. Thus the minimum number of excited state species per PSII-RC is seven (P_{680}, $Pheo_1$, $Pheo_2$, Ch_{acc1}, Chl_{acc2}, Chl_{ant1}, and Chl_{ant2}), taking P_{680} as one "pseudospecies". In addition, some of the RC particles contain also either one or both of the pigments Chl_{add2} or Chl_{add3}. Since the very small Chl_{add1} pool is of minor importance for the overall kinetics, it has been omitted in order to simplify the calculations. Thus for the actual modeling the sample consists of PSII-RCs containing 7, 8, or 9 pigments. On the basis of the spectral model, we took the

TABLE 1: Parameters for Radical Pair Formation As Obtained from the Model with Sequential RP Relaxation

	rate constant (ns^{-1})[a]	ΔG (meV)[b]	$1/\tau_{RP_i}$ (ns^{-1})[c]
$P_{680}^* \rightarrow RP_1$	700	−1.5	0.014
$RP_1 \rightarrow RP_2$	21	−7.7	0.025
$RP_2 \rightarrow RP_3$	2.1	−7.2	0.010
$RP_3 \rightarrow RP_4$	0.61	−11	0.013
$RP_4 \rightarrow RP_5$	0.13	−19	0.022

[a] Second column gives the rate constant for the reaction depicted in the first column. [b] Third column gives the ΔG value for the respective reaction. [c] Last column the intrinsic decay rates for the RPs.

probabilities of 0.13 and 0.15 for Chl_{add2} and Chl_{add3}, respectively, to be present in the PSII-RC.[28] To simulate an arrangement which lacks one or both of these chromophores, the respective spectra and rate constants were set to zero. For the modeling, the RP states also have such a "zero spectrum" (absorption and fluorescence), but in contrast to the above case not all the rate constants to the remaining states are equal to zero.

For modeling the fluorescence kinetics of the PSII-RC we use the parameters obtained from the spectral model that is described above. However, the kinetics is not entirely determined by the individual absorption and fluorescence spectra, but also depends upon parameters that are (i) connected to the Förster formula and (ii) associated with RP kinetics (eqs 1 and 2). Some of the constants in the Förster formula can be estimated from literature values. The radiative lifetime for a (hypothetical) isolated Chl in a protein surrounding can be calculated from the fluorescence lifetime of $\tau_j = 3$ ns[49−51] and the fluorescence quantum yield of 0.36[52] as $\tau_{0j} = 8.3$ ns. For P_{680} and Pheo radiative lifetimes of 4.2 and 12.5 ns, respectively, were assumed to take into account the different oscillator strengths of these pigments.[53] The refractive index n of the protein surrounding is taken as 1.34 (see ref 54 and references therein). The factors κ_{ij}^2/R_{ij}^6 in eq 5 will be called "structure factors" henceforth. The structure factors for the core pigments of the PSII-RC were calculated from the atomic coordinates of the *Rhodopseudomons viridis* RC,[55] as obtained from the Brookhaven protein data bank (file pdb1prc). To calculate the energy transfer rates between the putative Chl dimer P_{680} and the remaining pigments of the RC core, the spectrum of the dimer was used in eq 5 along with the larger one of the two structure factors of the special pair Chls (see Table 2). The remaining structure factors and the parameters associated with RP formation were regarded as adjustable parameters in the model and had to be fitted to the experimental data.

To describe the RP formation in the PSII-RC, we tested different mechanisms (see below). In one of these cases, the value of ΔG_{CS} had a Gaussian distribution.[22−24] To simulate the kinetics of this mechanism, the averaging over the spectral arrangements was combined with an averaging over RCs with different values of ΔG_{CS}. To account for a possible dependence of k_{CS} on ΔG_{CS}, we used the Marcus equation:[56,57]

$$k_{CS} = \frac{2\pi}{\hbar} H^2 \frac{1}{(4\pi\lambda RT)^{1/2}} \exp\left(\frac{-(\Delta G_{CS} + \lambda)^2}{4\lambda RT}\right) \qquad (12)$$

In this case the width of the ΔG_{CS} distribution was an additional adjustable parameter as were the reorganisation energy λ and the matrix element for electronic coupling H^2.

A major problem for the kinetic modeling of systems with inhomogeneously broadened spectra is the fact that the computer calculations become extremely time consuming. For this reason, the model parameters were not fitted directly to the original experimental data which would have required in addition a convolution with the response function of the apparatus in every iteration step. Instead, we analyzed the fluorescence decay curves in a first step globally as a sum of exponentials to obtain DAS and the corresponding lifetimes.[46] The results of this global analysis were then used to recalculate the deconvoluted decay curves, which in turn were used for comparison with the modeled decays (see above). As criterion for the quality of the fit, the weighted mean square deviation (denoted as χ^2) between these parametrized curves and the modeled fluorescence decays was taken.

$$\chi^2 = \frac{1}{M} \sum_{m=1}^{M} \frac{(y_m - y_m)^2}{y_m} \qquad (13)$$

In this equation, M is the number of data points for all different times and detection wavelengths. The Y_m are the experimental data (more exactly, the data calculated from the experimental lifetimes and their DAS) and y_m are the corresponding data as derived from the kinetic model. The fluorescence kinetics was analyzed simultaneously on three different time scales: $3 < t < 150$ ps (resolution 3 ps), $0.1 < t < 3$ ns (resolution 0.1 ns) and $0.7 < t < 20$ ns (resolution 0.7 ns). For the first two and for the third time scales, the fits were compared with experimental data analyzed in windows of 3.2 and 90 ns, respectively (see next paragraph). A single average χ^2 value was calculated over all three time scales.

As fitting procedure for the minimization of χ^2, we chose a genetic algorithm[28,58,59] as previously used for the spectral fitting.[28] The idea behind this algorithm is to transfer the principles of Darwinian evolution to the computer and to adapt it to problems of numerical optimization. Besides other advantages, this search procedure avoids getting trapped in local minima as other algorithms based on derivative evaluations often do, in particular in the case of such complex fitting problems as given here. Moreover, the allowed fitting range for each single parameter can be controlled in a straightforward manner so that no "unreasonable" results are obtained. For this work, a resolution of 6 bits/parameter was used together with a probability of 0.8 for crossing over and 0.01−0.03/gene and individual for mutation. The number of generations used for this fitting procedure was 50−100 and the population size was 3000 individuals/generation. In a preliminary run, only 300 spectral arrangements were averaged for each individual. After the genetic algorithm had approximately localized a χ^2 minimum, the calculations were stopped and the obtained results were used as starting values for a second "refinement run" where now 600 spectral arrangements were averaged. This procedure increases the speed of the calculations and the accuracy of the fitted parameters. A typical run of a genetic algorithm took about two weeks on a DEC 3000-800 computer.

Results

Fluorescence Kinetics of PSII-RCs at 77 K. The PSII-RCs were rapidly cooled in a 0.1 mm path length cell to 77 K and were excited at a wavelength of 650 nm. Fluorescence decay curves were recorded for several detection wavelengths between 675 and 690 nm. These data were analyzed globally to obtain the lifetimes and the corresponding DAS (see above). Figure 1 shows the result of such a global analysis for a time window of 3.2 ns. Five lifetimes were required to properly describe the decay curves, ($\chi^2 = 1.1$). The four slower components (43 ps, 220 ps, 1.6 ns, and ∼51 ns) have a similar spectrum peaking at about 682 nm. The longest lifetime is not well determined in this time window. Only the spectrum of the shortest-lived component (7 ps) is substantially different from the others, showing a positive−negative going shape with

TABLE 2: Structure Factors κ_{ij}^2/R_{ij}^6 (nm^{-6}) between the Chromophores of the PSII-RC As Obtained from the Model with Sequential RP Relaxation[a]

	P_{680} (14 710)[b]	$Pheo_1$ (14 703)	$Pheo_2$ (14 885)	Chl_{acc1} (14 855)	Chl_{acc2} (14 645)	Chl_{ant1} (14 950)	Chl_{ant2} (14 740)	Chl_{add2} (14 796)	Chl_{add3} (14 632)
P_{680} (14 710)	–	0.036[b]	0.032[b]	0.55[b]	0.69[b]	*c*	*c*	*c*	*c*
$Pheo_1$ (14 703)		–	0.0014[b]	0.0035[b]	0.83[b]	0.0024	*c*	*c*	0.0016
$Pheo_2$ (14 885)			–	0.77[b]	0.003[b]	*c*	*c*	0.0008	**0.013**
Chl_{acc1} (14 855)				–	0.016[b]	*c*	0.0083	0.0086	0.0093
Chl_{acc2} (14 645)					–	*c*	0.0031	**0.011**	0.0009
Chl_{ant1} (14 950)						–	0.0002	**0.013**	**0.01**
Chl_{ant2} (14 740)							–	0.0035	**0.014**
Chl_{add2} (14 796)								–	0.001
Chl_{add3} (14 632)									–

[a] Numbers in parentheses denote the IDF maxima (cm^{-1}) for each pigment. Structure factors indicated in bold denote pigment pairs with one partner outside the core which should have the closest spatial proximity. This table is symmetric with respect to its diagonal axis ($\kappa_{ij}^2/R_{ij}^6 = \kappa_{ji}^2/R_{ji}^6$). [b] Orientation factor is fixed from the RC structure of *Rhodopseudomonas viridis*. [c] Orientation factor is below 0.0001.

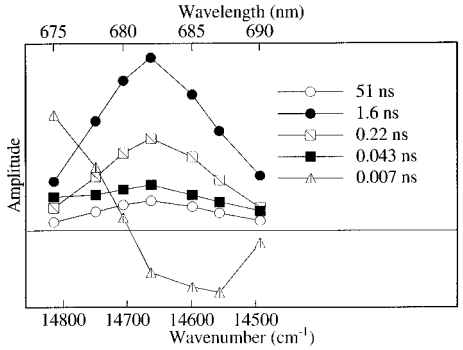

Figure 1. Fluorescence kinetics of PSII-RCs measured at different detection wavelengths at a temperature of 77 K and an excitation wavelength of 650 nm described as DAS together with the corresponding lifetimes. The time window used for these measurements was 3.2 ns with a time resolution of 2 ps/channel. An additional set of measurements over a time range of 90 ns is not shown.

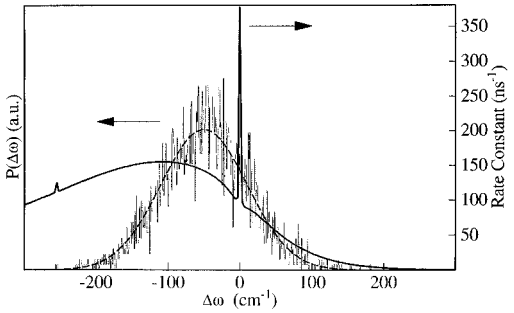

Figure 2. The noisy curve represents the distribution function $P(\Delta\omega)$ for the energy difference $\Delta\omega$ between the ZPLs of the acceptor pigment P_2 and the donor pigment P_1. It is calculated by taking 4000 pigment pairs at random from the two IDFs. The dashed line represents the same distribution function but calculated as cross correlation between the IDFs (both assigned to the left *y* axis). Also shown is the energy transfer rate (Förster rate) as a function of the energy difference $\Delta\omega$ between the ZPLs of donor and acceptor spectra (solid line, assigned to the right *y*-axis).

a zero crossing at about 680 nm. To better characterize the slower decay processes, the time-resolved fluorescence of the PSII-RCs was also measured in a time window of 90 ns (data not shown). The lifetimes obtained from these measurements were 69 ps, 600 ps, 2.2 ns, 5.7 ns, and 41 ns, again all with roughly the same spectrum peaking at about 682 nm. The χ^2 value of this analysis was 1.2. These data are quite similar to those reported earlier.[14,60]

Kinetic Simulations. *Effects of Inhomogeneous Broadening on the Energy Transfer*. The kinetic effects of inhomogeneous broadening in an energy transfer system are quite drastic. It is not possible to present these effects in a transparent manner for a system containing more than two pigments. For this reason we show some results for two inhomogeneously broadened pigment pools, P_1 and P_2 in a fixed relative orientation to each other. We assume that the coupling between these pigments is weak, so that the Förster theory can be applied to calculate the energy transfer rates (eq 5). For the following calculations the homogeneous 77 K−absorption and emission spectra of Chl are used.[28] We further assume that the spectra of these pigments are inhomogeneously broadened with an IDF fwhm of 100 cm^{-1}. In the first example, the IDF maximum of P_1 is at a 50 cm^{-1} higher energy than that of P_2, so that $P_1^* + P_2 \rightarrow P_1 + P_2^*$ is an energetic downhill reaction for most of the pigment pairs. However, due to the inhomogeneous broadening, the ordering of the energetic levels is inverted for part of the distribution.

We are interested in the dispersion of the rate constant $W_{2\leftarrow1}$ for energy transfer from P_1 to P_2 that is introduced into the system by the inhomogeneous broadening. Figure 2 shows the dependence of the energy transfer rate constant on the energy difference ($\Delta\omega$) between the P_1 and P_2 ZPLs (calculated with $n = 1.34$, $\tau_{01} = 8.3$ ns, and $\kappa_{ij}^2/R_{ij}^6 = 0.0018$). In case of negative energy differences (downhill reaction), this transfer rate is calculated according to eq 5, for the inverse case according to eq 7. (Note that the peak in this distribution is caused by the overlap of the zero phonon lines. It may not be adequate to take into account energy transfer between the zero phonon lines. The effect of this peak on the kinetic simulations in this work is negligible anyway, however.) Also depicted in Figure 2 is the probability distribution $P(\Delta\omega)$ for the energy difference between the ZPLs of both pigments. The "noisy" distribution function results from a random choice of 4000 discrete pigment pairs out of the IDFs (such a random choice will also be used for the fitting of the kinetics in the next section). The dashed curve also shows this distribution function $P(\Delta\omega)$ but calculated analytically as the cross correlation of the two IDFs.

$$P(\Delta\omega) = \int_0^\infty \mathrm{IDF}_1(\omega)\mathrm{IDF}_2(\omega+\Delta\omega)\,\mathrm{d}\omega \qquad (14)$$

Figure 3 shows the resulting distributions for the energy transfer rate constant for an energy difference between the IDF maxima of -50 cm^{-1} (thick solid) and -300 cm^{-1} (thick dashed), respectively. Again the noisy curve is from the random choice of 4000 pigment pairs and the solid line is the distribution function that can be calculated analytically from eq 14 together with the rate constant function shown in Figure 2. It can be seen that the inhomogeneous broadening of the pigment spectra introduces a pronounced dispersion for the energy transfer rate constants and that the shape of this dispersion depends critically upon the energy difference between the maxima of the IDFs.

Modeling the Fluorescence Kinetics of the PSII-RC. The 77 K fluorescence kinetics of the PSII-RC was fitted to the kinetic model described in the previous sections. It includes inhomo-

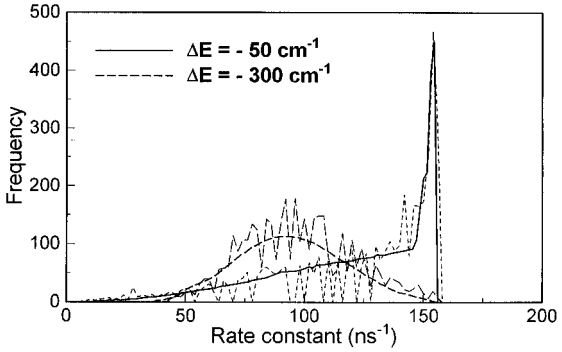

Figure 3. Frequency distribution of the energy transfer rates for the model system consisting of 4000 pairs of pigments as described in the text. The figure shows the transfer rates for the reaction $P_1^* + P_2 \rightarrow P_1 + P_2^*$. The energy difference between the IDF maxima of both pigments is -50 cm^{-1} (thick full line) and -300 cm^{-1} (thick dashed), respectively.

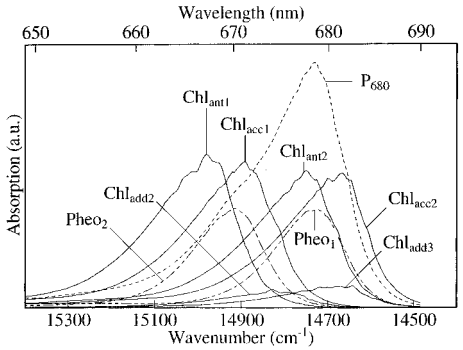

Figure 4. Spectral decomposition for the absorption spectrum of the PSII-RC according to ref 28. The inhomogeneously broadened spectra of the single pigments are calculated by averaging 600 homogeneous absorption profiles taken at random from the corresponding IDFs. The noise on the spectra is caused by this random choice. For details see text.

geneous broadening and sample heterogeneity and uses the results of the model developed earlier for the PSII-RC absorption spectrum.[28] In all calculations described in the following text, 600 different spectral arrangements were used to describe the kinetics. If not stated otherwise, the fluorescence kinetics was fitted simultaneously in three different time windows: $3 < t < 150$ ps, $0.1 < t < 3$ ns, and $0.7 < t < 20$ ns. In order to prove that the kinetic model is consistent with the spectral model, the homogeneous absorption spectra of all spectral arrangements used in the calculations were summed up. As shown in Figure 4, the decomposition of the PSII-RC absorption spectrum from our previous spectral analysis[28] is obtained in good approximation. The noisy outlook of these spectra is caused by the random choice of the spectral arrangements. With an increasing number of arrangements the spectra become smoother.

Single Radical Pair and Energy Distribution. In a first approach we tested the simplest possible mechanism of RP formation which is illustrated in Figure 5A. According to this mechanism, the formation of the RP proceeds in a single step and the free energy difference for charge separation ΔG_{CS} is the same for every PSII-RC in the sample. The quality of the corresponding fits was extremely poor (data not shown).

In a second step, the model was modified such that the free energy difference for charge separation ΔG_{CS} had a Gaussian distribution (see Figure 5B). To account for a dependence of the charge separation rate, k_{CS} on the value of ΔG_{CS} eq 12 was applied. Using this model, the correspondence between the calculated decay curves and the experimental fluorescence kinetics could be improved substantially. Nevertheless, also in this case severe deviations between experiment and model

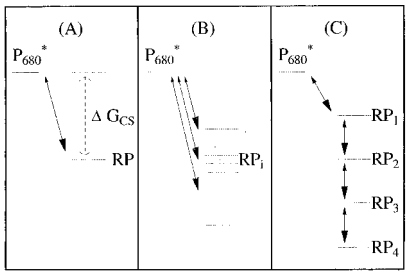

Figure 5. Different mechanisms of radical pair formation in the PSII-RC: (A) one-step mechanism, the free energy difference for charge separation (ΔG_{CS}) is the same for all RCs in the sample; (B) one-step mechanism with a static distribution of ΔG_{CS}; (C) sequential radical pair relaxation.

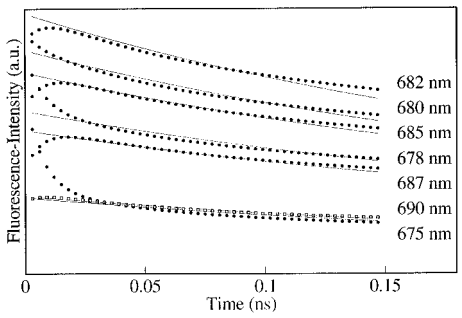

Figure 6. Calculated fluorescence decay curves obtained from the experimental lifetimes and corresponding DAS (dots). Also shown are the respective fitted curves (solid lines) as obtained from the kinetic modeling by using the model with a static distribution of free energy difference for charge separation (model B in Figure 5).

became apparent, especially for times between 3 and 150 ps (data not shown). We therefore analyzed this time range separately, neglecting the two longer time windows. The resulting fits are shown in Figure 6 where the "experimental" data are depicted together with the fluorescence decay curves which were calculated from the kinetic model. As can be seen, even if only this short time window is analyzed separately no acceptable correspondence to the experimental data could be obtained. Especially for times shorter than 20 ps, substantial deviations between corresponding curves become apparent. The shape of the fitted decay curves is largely determined by the majority of the data points (between about 30 and 150 ps) which show a quite "flat" time course so that the rise and decay components at earlier times can not be described within the framework of this model. Thus it can be stated, that also the kinetic model with a static Gaussian distribution of ΔG_{CS} is not suitable to describe the fluorescence kinetics of the PSII-RC at low temperatures. For completeness, some parameters obtained from this model shall be given, although taking the very poor quality of the fits into account they do not have any physical meaning: The distribution of ΔG_{CS} was centered at -105 meV with a fwhm of 17 meV and the reorganization energy λ was 120 meV. These parameters give rise to a distribution for k_{CS} centered at 16 ns^{-1}, whereas the highest possible value of the charge separation rate in this fit was about 40 ns^{-1}.

Sequential Radical Pair Relaxation. As a third alternative we tested a model with sequential RP relaxation (Figure 5C). In this model a primary radical pair RP_1 is formed from the excited primary electron donor P_{680}* with a rate constant k_{CS}. RP_1 is located lower in energy by ΔG_1 than P_{680}* and it relaxes to a secondary state RP_2 with a rate contant k_{RP2}. RP_2 is located by ΔG_2 lower in energy than the first one. Thus a whole series of RPs with decreasing energy can be included into the model. Each RP state can react back to the previous one with a rate constant that can be calculated from eq 7 with the corresponding

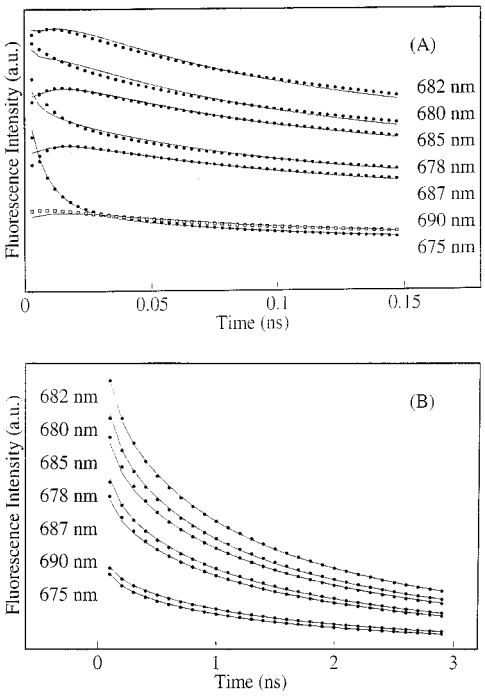

Figure 7. The same as that in Figure 6 but for the model with sequential radical pair relaxation (model C in Figure 5). Figures 7A,B show the results for two of the three different time windows which were included in the analysis. The long-time window, where no significant deviations occur between model and experiment, is not shown.

values of ΔG_i and k_{RP_i}. RP_1 can recombine back to P_{680}*, giving rise to delayed fluorescence.

The resulting fits for this model are shown in Figure 7 for time windows of 150 ps (A) and 3 ns (B). The quality of the fits is drastically improved as compared to the previous model with a static distribution of ΔG_{CS} (see Figure 6). The long time range (above 150 ps) is fitted perfectly. Even in the short time range of up to 150 ps only minor deviations occur. Five sequential RP states were included in this model. For the kinetic modeling described here, the IDF maxima of the homogeneous absorption and fluorescence spectra were slightly shifted as compared to the results of our spectral study. These spectral shifts of the IDF maxima are less than 0.5 nm for each pigment but nevertheless they improve the quality of the fits. Note that we also allowed for spectral shifts in the previous two models that did nevertheless not fit the data.

The parameters calculated for charge separation and RP relaxation are collected in Table 1. According to these results, the charge separation occurs from P_{680}* with a rate constant of 700 ns^{-1} and a free energy difference of only $\Delta G_1 = -1.5$ meV. The relaxation steps of the RPs proceed on a much slower time scale with an increasing lifetime of the consecutive RP states. The free energy differences between the following RPs are in the order of roughly −10 meV and these states decay with rate constants $1/\tau_{RP_i}$ of about 0.01 to 0.025 ns^{-1}. The structure factors for the pigments of the PSII-RC are depicted in Table 2. Note that this table is symmetric with respect to its diagonal axis. The structure factors for the PSII-RC core were taken from the RC of *Rhodopseudomonas viridis* (see above), whereas those for the antenna and additional Chls were obtained by fitting the model to the experimentally observed fluorescence kinetics. The largest of these fitted values are in the range of 0.01 nm^{-6}, which is similar to the lowest structure factors inside the RC core. However, they are in their large majority far below the values of the core, some of them are even close to zero. This means that the Chl_{ant} and Chl_{add} are not located closely to their neighbors and/or have an orientation that is not very favorable for energy transfer.

The structure factors of Table 2 were used to calculate the average rate constants for energy transfer. Due to the inhomogeneous broadening of the spectra these rate constants show a pronounced dispersion, some examples for the corresponding distribution functions are shown in the previous section (see Figure 3). The mean values of these energy transfer rate constants (forward and backward rates) are given in Table 3. The fastest energy transfer processes occur in the RC core with calculated rate constants in the order of up to 10^5 ns^{-1}. Such high rate constants are probably out of range for application of the Förster formula. However, since lifetimes of shorter than 1 ps are not considered for the calculation of the simulated fluorescence kinetics due to limited experimental resolution, the exact value of these rate constants is of no further importance in this context. We note that, only if the structure factors of the RC core were lowered by more than 1 order of magnitude, the quality of the fits would be influenced by the change of the corresponding rate constants, but such large deviations are quite unlikely. Energy transfer reactions with participation of antenna or additional Chls are generally several orders of magnitude slower than the equilibration processes inside the RC core. Nevertheless, also for these pigments average rate constants of up to 1200 ns^{-1} were calculated in some cases. Since from Table 3 it is difficult to obtain a detailed picture of the complex energy transfer kinetics within the PSII-RC, it is helpful to present the time course of the populations of electronically excited pigments.

These populations for the chromophores in the complex are shown in Figure 8. Once again these data represent an average over 600 spectral arrangements. Immediately after excitation of the sample at time $t = 0$ with a light flash of 650 nm, some very fast energy equilibration processes take place. This is the reason why a large part of the energy gets located rapidly on the low-energy pigments Chl_{acc2}, $Pheo_1$, P_{680}, Chl_{add3}, and Chl_{ant2}. The depopulation of the more blue absorbing pigments $Pheo_2$, Chl_{acc1}, and Chl_{add2} happens also on this fast time scale so that they practically do not contribute at longer times. For this reason the time courses for these three pigments are not shown in Figure 8. The excited state of Chl_{ant1} decays with lifetimes of roughly 10 ps, which is due to energy transfer processes towards the low energy pigments Chl_{acc2}, $Pheo_1$, and P_{680}.

It has been pointed out already that due to inhomogeneous broadening the fluorescence kinetics has to be described by a complex lifetime-distribution $a(\lambda_{exc},\lambda_{em},\tau)$, rather than by a sum of exponentials (eq 10). This lifetime distribution is presented in Figure 9 for detection wavelengths of 675 and 685 nm, respectively (note the splitting of the time scale). Certain regions of this distribution can be roughly assigned to the underlying processes in the PSII-RC. The leftmost peak in Figure 9 shows a positive amplitude at 675 nm and a negative one at 685 nm and represents the fast (below 1 ps) energy transfer processes in the PSII-RC core which were not resolved in our experiments. The following region of 2 to 4 ps can be attributed essentially to the formation of RP_1 from P_{680}*. Also between 5 and 15 ps the amplitudes of the distribution change their sign for the different detection wavelengths. This region shows a pronounced dispersion due to the inhomogeneous broadening, and it can be mainly assigned to energy transfer from Chl_{ant1} toward the red-absorbing pigments (see also Figure 8). The relaxation from RP_1 to RP_2 and from RP_2 to RP_3, respectively, is responsible for the occurrence of the two peaks in the lifetime distribution at around 0.1 and 0.6 ns. Nevertheless, also in this lifetime range the influence of inhomogeneous broadening is reflected by the dispersion of the distribution. This

TABLE 3: Average Value (First Moment) of Rate Constants for Energy Transfer (ns^{-1}) between the Chromophores of the PSII-RC As Obtained from the Model with Sequential RP Relaxation[a]

	P_{680} (14 710)[a]	$Pheo_1$ (14 703)	$Pheo_2$ (14 885)	Chl_{acc1} (14 855)	Chl_{acc2} (14 645)	Chl_{ant1} (14 950)	Chl_{ant2} (14 740)	Chl_{add2} (14 796)	Chl_{add3} (14 632)
P_{680} (14 710)	–	3000[b]	3200[b]	86000[b]	47000[b]	1	0	7	2
$Pheo_1$ (14 703)	2900[b]	–	45[b]	180[b]	19000[b]	89	1	0	38
$Pheo_2$ (14 885)	200[b]	3[b]	–	26000[b]	3[b]	1	0	11	4
Chl_{acc1} (14 855)	4200[b]	17[b]	37000[b]	–	46[b]	9	56	250	24
Chl_{acc2} (14 645)	94000[b]	49000[b]	120[b]	1200[b]	–	5	240	940	48
Chl_{ant1} (14 950)	0	2	0.4	3	0	–	0.4	100	2
Chl_{ant2} (14 740)	0	1	0.2	770	88	15	–	270	350
Chl_{add2} (14 796)	2	0	46	740	75	1200	110	–	9
Chl_{add3} (14 632)	5	86	480	700	55	570	1100	77	–

[a] Numbers in parentheses denote the IDF-maximum (in cm^{-1}) for each pigment. [b] Energy transfer rate in the core PSII-RC.

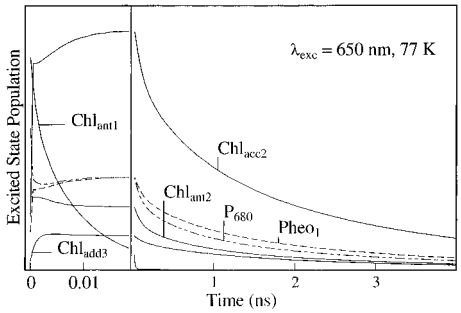

Figure 8. Time course of the excited state populations for the pigments in a sample of PSII-RCs after irradiation with a 650 nm flash at a temperature of 77 K. The population of the pigments which are not shown are close to zero for times longer than 1 ps. Note the splitting of the time scale.

becomes most apparent for lifetimes around 0.6 ns because the depopulation of Chl_{acc2} (red "trap" Chl) proceeds on this time scale as can be seen from Figure 8. The lifetime distribution exhibits three additional maxima in the range of several ns which are positive for all detection wavelengths and show only little dispersion (data not shown). These maxima are assigned to the relaxation of RP_3 (∼2 ns) and RP_4 (∼8 ns) and to recombination fluorescence from P_{680} (45 ns).

Predictions from the Kinetic Model. *Temperature Dependence of Stationary Emission Spectra.* Using the parameter set of the radical pair relaxation model that was optimized for a temperature of 77 K and an excitation wavelength of 650 nm (structure factors, free energy differences, and forward rate constants), the stationary emission spectrum can be obtained from our kinetic model for a limited temperature range (see eq 11). In particular we are interested what the model predicts for the temperature dependence of shape and maximum of the fluorescence spectrum, as well as for the fluorescence quantum yield. These parameters are easily accessible experimentally. For these calculations the temperature dependence of the homogeneous spectra in the complex was also taken into account, the forward rate constants were taken from the sequential radical pair model, and the backward rates were calculated according to eq 7. The relative fluorescence quantum yield was obtained by integrating the emission spectra. As the result of these calculations, the temperature dependence of the stationary fluorescence spectrum is shown in Figure 10. At 32 K the maximum of the spectrum is located at 685 nm. If the temperature is raised the fluorescence quantum yield increases, the spectrum broadens and its maximum shifts slightly to the blue. For temperatures lower than 32 K, the spectrum essentially keeps its shape and the fluorescence quantum yield again increases. This temperature dependence of the quantum yield is shown in the inset of Figure 10 (an explanation for these phenomena is given in the Discussion section).

Time Course of Excited Chromophores upon Excitation at 685 nm for Different Temperatures. In Figure 11A, the excited state populations for the pigments in the PSII-RC are calculated for an excitation wavelength at the red edge of the absorption spectrum (685 nm), again by using the forward rates that have been obtained from the sequential radical pair model. After a very fast equilibration that is essentially finished after 2 ps, all of the pigments are close to thermal equilibrium. The excited state populations of the pigments that absorb on the blue side of the spectrum (like Chl_{ant1}) are almost zero after this fast equilibration has taken place. This is the reason why they are not depicted in Figure 11A. A further decrease in the temperature from 77 K enhances the localization of excitation energy on the very red-absorbing chromophores in the PSII-RC even more. This is shown in Figure 11B where the time course of the populations is shown which is calculated for an excitation wavelength of 685 nm and a temperature of 20 K (using the same forward rates as in Figure 11A). Under these conditions, Chl_{acc2} and Chl_{add3} act as trap states and are practically the only excited species for times longer than 25 ps.

Discussion

In a previous study we presented a model to explain the temperature dependent shape of the PSII-RC absorption spectra.[28] This model is based on the theoretical calculation of spectral line shapes for the pigments in the complex using the theory for electron−phonon coupling[29,30] and it takes into account the inhomogeneous broadening of the spectra. With the exception of the putative Chl dimer P_{680}, the model assumes weak coupling between the pigments in the PSII-RC so that excitonic coupling can be neglected. We obtained a decomposition for the absorption spectrum of the PSII-RC. In the present work we used and extended that model to analyze the fluorescence kinetics of the PSII-RC at 77 K. Similar approaches have been used in the past to describe the absorption and fluorescence kinetics of pigment−protein complexes from photosynthetic bacteria.[61−63]

A basic feature of our model is that it uses the Förster formula to calculate the energy transfer rates between two pigments. Strictly speaking this equation is only valid in the weak coupling limit. However, there now exists experimental evidence for the validity of this formula up to energy transfer rates of at least 1500 ns^{-1}.[54,64] These findings are supported by theoretical investigations of Knox et al.[43] which indicate that the Förster formula might also hold in the case of a strong coupling between the energy donor and acceptor. We thus feel confident to apply this formula for the calculation of the rate constants for energy transfer outside the core RC. For these pigments most of the calculated rates are far below the value given above (see Table 3). This is, however, not the case for the rates that were calculated for energy transfer among the core pigments. Most of these numbers for the forward rates are probably out of range for application of the Förster formula. However, since these equilibration processes are beyond the time resolution of our

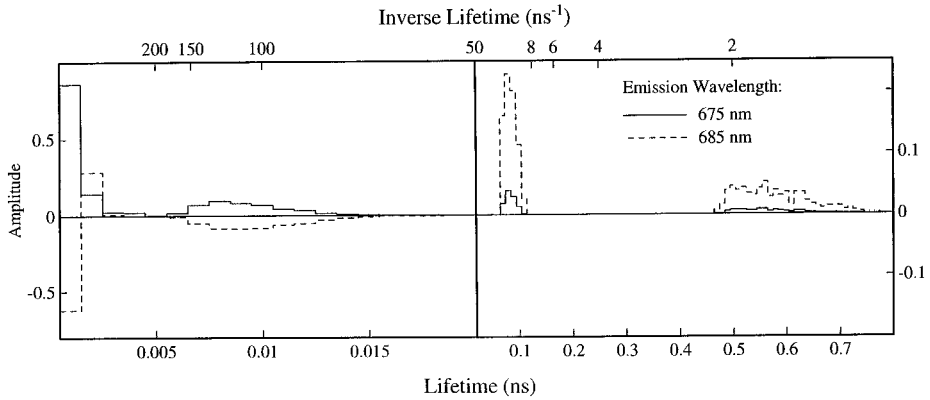

Figure 9. Lifetime distributions obtained from the kinetic modeling for detection wavelengths of 675 and 685 nm using the model with sequential radical pair relaxation. Note the splitting of the time scale. For details see text.

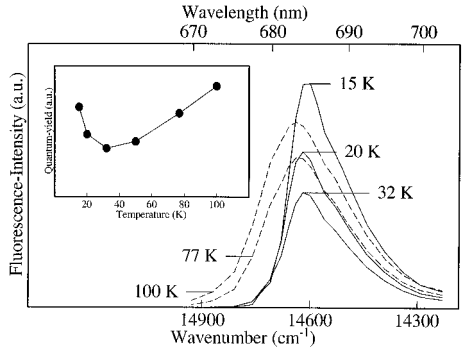

Figure 10. Temperature dependence of the stationary fluorescence spectrum calculated by using the kinetic model with sequential radical pair relaxation. The inset shows the relative fluorescence quantum yield as a function of temperature which is obtained by integrating the respective fluorescence spectra.

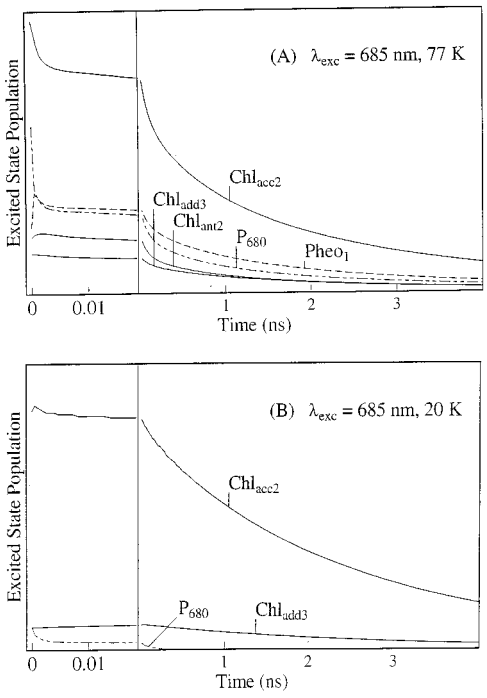

Figure 11. Time course of excited state populations in the PSII-RC at 77 K (A) and at 20 K (B) calculated for an excitation flash of 685 nm. The population of the pigments which are not shown are close to zero for times longer than 1 ps. Note the splitting of the time scale. For details see text.

experimental data and lifetimes of less than 1 ps were thus not considered in the fitting procedure anyway, this poses no problem for the kinetic modeling performed in this study. Nevertheless, it should be pointed out that sub-picosecond processes have been observed in the PSII-RC which can be interpreted as such an ultrafast energy equilibration in the core RC.[17,26,65] Thus in our opinion it is justified to assume that energy transfer within the RC core cannot be detected with the time resolution given in our measurements. For this reason it is quite justified that the structure factors for the pigments in the core RC were taken from the X-ray structure of the bacterial RC, despite the experimental evidence that the detailed structure of the two systems differs substantially.[28,36]

Inhomogeneous spectral broadening is a general feature of photosynthetic pigment−protein complexes which becomes apparent especially at low temperatures.[48,62,66,67] In this study we showed that inhomogeneous broadening in a pigment complex introduces a pronounced dispersion in the rate constants for energy transfer. The resulting distribution functions for the rates are generally rather broad and may be strongly asymmetric, depending on the energy difference of the IDFs of donor and acceptor spectrum as can be seen from Figure 3. Thus it is not appropriate to describe the energy transfer processes with just one single rate constant. Rather for kinetic modeling of such a complex system the rate dispersion has to be taken into account.

According to this study the outer pigments (Chl$_{ant}$ and Chl$_{add}$) are responsible for the relatively slow energy transfer processes in the range between 5 and 30 ps that have been observed experimentally by several workers.[14,17,18,68,69] From Figure 8 it is obvious that according to the kinetic model in particular Chl$_{ant1}$ is important in this respect. It has its absorption maximum on the high energy side of the Q_y region of the PSII-RC spectrum. Its depopulation proceeds on the timescale mentioned above due to the energy transfer to low-energy pigments. Chl$_{ant1}$ can be removed by biochemical methods. The resulting samples have a pigment ratio of approximately 5 Chl/2 Pheo and do no longer show the above mentioned energy transfer processes.[69] These experimental findings strongly support the model which is presented in this work.

Spatial Arrangement. According to the structure factors for energy transfer given in Table 2, the pigments in the entire RC can be grouped in "inner" pigments (pigments of the RC core which are connected by very large structure factors, see Table 2), and "outer" pigments, which are the antenna and additional Chls. This is in very good agreement with the structural picture that we already suggested on the basis of our spectral model.[28] Furthermore, it is in agreement with the computer modeling studies of Ruffle et al.[37] In that work it is proposed that the His-118 amino acid residues on both the D_1 and D_2 polypeptides, which are probably located on the outside of the protein complex, could serve as binding sites for the antenna Chls. From the structure factors obtained from the kinetic model the distances between the outer Chls and the remaining pigments can be estimated. The largest structure factors are in the range

of 0.01 nm^{-6}, this corresponds to distances $R_{ij} \geq 2$ nm (by assuming a value of $\kappa_{ij}^2 = {}^2/_3$, which is obtained by averaging over all possible orientations of donor and acceptor molecules). Distances in this range are in accordance with the suggestions of Schelvis et al.[70]

Charge Separation and Radical Pair Kinetics. An important question concerns the mechanism of radical pair formation in the PSII-RC. A model with a single radical pair failed completely. In a second approach we tried to fit the data to a model that includes a static Gaussian distribution of the free energy for charge separation. Such a mechanism was suggested for bacterial RCs[22,23] and also for the PSII-RC.[24] An important result of this study is that such a model could not be fitted to our low-temperature time-resolved data either, even in the case when only the time range of up to 150 ps was analyzed. One reason for this could be that for the calculations the Marcus formula was applied which is known to be valid only in the high-temperature limit.[56] In our view this seems not to be very likely, since it should at least be possible to approximate the dependence of k_{CS} on ΔG_{CS} in a reasonable way by a classical "Marcus-type" expression. For our calculations a Gaussian distribution function for ΔG_{CS} was used. It might be possible to describe the fluorescence kinetics by assuming a more complex distribution function (e.g., with more than one maximum), but any such calculations would be highly speculative.

In order to better describe the fluorescence kinetics, the model was modified in a way that an "unrelaxed" RP_1 is formed as product of the charge separation process. Relaxation of this RP_1 takes place via a series of RP states, each one lying lower in energy than the previous one. The relaxation can be envisaged to be brought about by small movements of the chromophores and changes in the protein conformation. Using this model we obtained a much better correspondence between the modeled decay curves and the experimental fluorescence kinetics. However, it might be misleading to interpret this sequential relaxation as a true step by step reaction with well-defined intermediate states. Probably it is more adequate to picture this reaction as a continuous process where the protein matrix reacts to the electrostatic forces caused by the sudden creation of a pair of ions. In this sense, the series of radical pairs with well-defined energy differences might be only a crude approximate description of what really happens inside the protein. This view is in accordance with the "dynamic solvation model" that has been suggested recently by the group of Woodbury and co-workers for bacterial RCs[25] and with femtosecond studies from our group.[27] Such a model implies that the free energy difference for charge separation becomes time dependent, rather than being a static value. According to Table 1 the formation of RP_1 is accompanied with a free energy change of only -1.5 meV (i.e., this state is almost isoenergetic with P_{680}*). With such a small energy gap the charge-separated state can recombine even at low temperatures, giving rise to recombination fluorescence. In this respect the conformational changes of the protein play a crucial role for the process of RP formation because the decrease in the free energy of the RP leads to a stabilization of the charge-separated state. The further the RP relaxation proceeds the less likely it is that a charge recombination takes place because with a growing energy gap the recombination becomes increasingly slower (see eq 7). By this relaxation process the energy gap is gradually increased up to -46 meV at long times (several tens of ns). This energy difference between P_{680}* and the final RP state (RP_5) in our model is in reasonable agreement to the values of ΔG_{CS} that have been estimated in the literature for the PSII-RC at 77 K.[14,24,71] However, it can not be excluded that the RP relaxation—and hence also the increase of the energy difference—is not yet completed on the time range that was accessible in the present study.

The sequential RP relaxation model could also be complicated further by introducing distributed energy levels for the single states. Using such a model did not improve the quality of the fits, however. We also should like to point out the possibility of a sequential electron transfer (e.g., that (P_{680}^+ Chl^-) is formed prior to (P_{680}^+ $Pheo^-$)) as was suggested for bacterial RCs.[72] Since RP states are not emitting fluorescence, time-resolved fluorescence spectroscopy will be of little help to answer the question of sequential electron transfer in the PSII-RC. Thus it cannot be excluded that, for example, RP_1 and RP_2 differ in their electron localization.

In the framework of the kinetic model a rate constant for primary charge separation of 700 ns^{-1} was calculated. One has to keep in mind that this value is not very precisely determined, due to the fact that the experimental fluorescence was only considered for times longer than 3 ps. The error in this fitting parameter can be estimated to be about ± 300 ns^{-1}. However, it should be pointed out that this freely fitted value for k_{CS} is in accordance with the 1.9 ps (corresponding to ~ 530 ns^{-1}) that has been measured for the excited state lifetime of P_{680} at 4.2 K by hole-burning spectroscopy.[34] Recently, a similar lifetime was attributed to the charge separation rate on the basis of transient absorption measurements at 77 K by Visser et al.[73]

As can be seen from Figures 7A,B, an acceptable fit quality could be obtained with the model described above over a large time range. However, especially for times shorter than about 20 ps, there are some deviations between the fitted curves and the ones that are calculated from the experimental lifetimes and the corresponding DAS. To judge the significance of these deviations one has to take into account that this time region may be affected by some systematic error due to the overlap with the apparatus response function (which had a fwhm of about 30 ps) and the difficulty of measuring in a cryostat. But even if these possible effects are considered, the deviations are still too large to regard the modeled curves in Figure 7A as a "perfect" fit. Another reason for these deviations could be the error that is introduced by using an excitation wavelength of 650 nm, whereas strictly speaking the decomposition of our spectral model is only valid down to about 655 nm. To clarify whether that might be the reason for this problem, we fitted the elements of the excitation vector $\mathbf{x}(t=0)$, which defines the initial conditions for the system of coupled differential equations (see eq 4), as free parameters. Since this did not improve the quality of the fits we can rule out the possibility that this is the cause of the deviations. One further possibility would be that the kinetics in this time range is influenced by "slow" energy transfer processes in the core RC, in particular by energy transfer from the blue Chl_{acc1} towards low-energy pigments. As was already pointed out, such a possibility seems not very likely, but we nevertheless tried to analyze the data with the structure factors of the core pigments as free fitting parameters. Also with this approach the quality of the fits could not be improved. Finally we consider the spectral decomposition on which we based our calculations as possible reason for the observed deviations. It cannot be excluded that the IDFs and also the shape of the homogeneous spectra differ from the real situation to a certain extent, even though our model in general describes the spectral properties of the PSII-RC very well. Having excluded most other reasons as causes of the still existing deviations between experimental and model curves at short times, we suggest that these deviations between experimental and model curves at short times are likely to be caused by some small but nevertheless significant correlation between the IDF functions of neighboring pigments.

Our model assumes uncorrelated zero phonon energies of all pigments, as is essentially supported by the hole-burning measurements. However, the information from the hole-burning measurements may not be precise enough in this complex system to really determine the amount of correlation precisely. Thus there is some room for improvement in the model by taking into account some limited amount of IDF correlation, although in practice this will be quite a difficult problem to treat.

Predictions of the Spectral Model for Different Excitation Wavelengths and Different Temperatures. For the PSII-RC the temperature dependence of the stationary fluorescence including the fluorescence quantum yield has been investigated by Groot et al.[24] Their data are in good qualitative agreement to what is calculated from our kinetic model (Figure 10). However, the experimentally observed minimum of the fluorescence quantum yield is located at 60 K, rather than at around 30 K. These discrepancies are likely to be caused by the intrinsic temperature dependence of the forward rates for RP relaxation which was not taken into account in the present study. On the basis of our modeling, we in principle agree with the general explanations of the observed temperature dependent phenomena which were given in the work of Groot et al.[24] However the important effects of inhomogeneous broadening were not considered in that work and furthermore a static ΔG distribution does not fit our data. Due to the Boltzmann principle the population of excited pigments on the blue side of the Q_y band increases if the temperature is raised. Fluorescence from these pigments broadens the emission spectrum on the blue side, shifts the fluorescence maximum to shorter wavelengths and increases the fluorescence quantum yield. In contrast at very low temperatures part of the excitation energy is trapped on pigments having their ZPLs at lower energies than P_{680} so that this energy can not be utilized for charge separation. Due to these "red" pigments the fluorescence quantum yield again increases. Of special importance in this respect is Chl_{acc2}. As can be seen from Figure 8 this pigment is the dominant emitting species at 77 K. Its population decays with lifetimes of roughly 0.6 ns. However, the average energy gap between Chl_{acc2} and P_{680} is small enough so that back transfer is still possible for a part of the PSII-RCs at this temperature.

Now we shall discuss the effects of temperature on the excited state populations in the PSII-RC upon excitation at 685 nm. From Figure 11A it is obvious that after excitation at the red edge of the spectrum at 77 K the fluorescence spectrum contains contributions from "Chl-type" pigments (including P_{680}) as well as a relatively high contribution from $Pheo_1$. Since the maximum of the inhomogeneously broadened $Pheo_1$ spectrum is at around 680 nm (see Figure 4) it should be possible to reduce this Pheo contribution by further lowering the temperature. This effect is demonstrated in Figure 11B where it is shown that, at 20 K the excitation energy is almost exclusively located on the trap states Chl_{acc2} and Chl_{add3}, the contribution of $Pheo_1$ to the overall population becomes negligible. This prediction is in full accordance with results of Kwa et al.[13] who, by fluorescence site-selection experiments, found that at liquid helium temperatures and upon long wavelength excitation the emission of the PSII-RC indeed is dominated by Chl-type pigments. In contrast, site-selection experiments at higher temperatures should slow the predicted contribution of Pheo to the emission of the PSII-RC. This was indeed observed in recent experiments (Konermann et al. Biochemistry submitted for publication) and provides strong support for the concepts and results from this work.

Conclusions

The aim of this modeling study was to describe the fluorescence kinetics of the PSII-RC by a consistent and physically reasonable model that includes inhomogeneous broadening and heterogeneity effects of the pigment composition in the sample. The kinetic model used for this purpose is based on the spectral model we presented earlier. We regard the fact that the kinetics are described quite well as an additional support for the validity of the concepts that we used for the decomposition of the absorption spectrum. The structural picture of a RC core that is surrounded by external Chls, which we suggested on the basis of the spectral model, gains support by the kinetic modeling carried out in this work. This study furthermore has important implications for the understanding of the mechanism of RP formation in the PSII-RC. The occurrence of sequential RP states can be interpreted as a dynamic relaxation process of the protein matrix that is triggered by the sudden creation of a pair of ions. We cannot entirely rule out a dispersive charge separation rate. However, the results presented here seem to indicate that a dispersive charge separation kinetics, if at all relevant, plays a minor role as compared to protein coupled RP relaxation for determining the fluorescence kinetics. This picture is fully in line with recent data on the behavior of purple bacterial RCs.[25−27]

Finally, one has to ask the question as to the uniqueness and/or error range of the individual parameters derived in this model. Such information is contained in the specific parameter distribution for the 3000 individuals making up a generation in the GA run. While a few of the parameters may have a relatively large error (like e.g., the primary charge separation rate, and the energy transfer rates within the core, see above) others have quite narrow error margins. Within the model (radical pair relaxation) both the energy transfer rates from the external pigments and the rates and free energy differences of the radical pairs have very small error ranges, typically less than 10−20% (i.e., the model is very stiff and small variations in these parameters lead to a poorer fit). This can be understood by the fact that for energy transfer the inhomogeneous broadening implies rather complex rate distributions for a given pair which can only be fulfilled within a very narrow range of structure factors. A similar reason holds for the RP parameters (rates and ΔG values). These parameters critically control the amount of long-lived fluorescence and their lifetimes, which are known very accurately from the fluorescence data. Overall this means that within the model the important parameters have rather narrow error ranges.

The model is able to make a variety of very detailed predictions as to the outcome of experiments that can be tested in detail. Several such predictions, such as the temperature dependence of the fluorescence spectra and yield, the results of fluorescence site-selection experiments, etc. have been verified quite independently already. Further predictions will be tested in the future experimentally. On the basis its ability to describe a variety of independent experimental data, the model so far performs very well. Improvements in the parameters may be possible if significant deviations with experimental data would appear, but so far we are not aware of any such deviating experimental results. Finally, it should be remarked that in order to describe the entire set of experimental fluorescence lifetime data used in this modeling (two sets of DADS measured over two time ranges), a total of 80 parameters (70 amplitudes and 10 lifetimes) were required. Our most complex model (Figure 5C) in contrast contains only 41 free fitting parameters (49 parameters if one takes into account also the minor spectral shifts of $\leq$0.5 nm as compared to the spectral model[28]). Thus the model presented here is successful in describing the kinetic data with a substantially smaller number of free parameters than is required for describing the underlying experimental fluorescence kinetics. This may serve as a convincing argument that the

model is not too complex (i.e., it does not contain too large a number of free parameters). If it had too may free parameters (i.e., if it were underdetermined by the data), it would most likely loose its ability to distinguish between different kinetic models, which is not the case (see above), and furthermore a variety of alternative "good" parameters sets describing the data would appear, which is also not the case.

Acknowledgment. We thank T. Pullerits from the University of Lund, Sweden, for the computer program EMST that was used to calculate the homogeneous lineshapes of the pigments. M. Reus from our group is acknowledged for the expert preparation of the PSII-RCs. This work was supported in part by the Deutsche Forschungsgemeinschaft, Sonderforschungsbereich 189, Heinrich-Heine-Universität Düsseldorf and Max-Planck-Institut für Strahlenchemie. We also thank Prof. K. Schaffner for his interest and support of this work.

References and Notes

(1) Nanba, O.; Satoh, K. *Proc. Natl. Acad. Sci. U.S.A.* **1987**, *84*, 109.
(2) Renger, G. In *The Photosystems: Structure, Function and Molecular Biology*; Barber, J., Ed.; Elsevier: Amsterdam, 1992; p 45.
(3) Barber, J. *Biochem. Soc. Trans.* **1994**, *22*, 313.
(4) Holzwarth, A. R.; Roelofs, T. A. *J. Photochem. Photobiol. B* **1992**, *15*, 45.
(5) Seibert, M. In *The Photosynthetic Reaction Center*; Deisenhofer, J., Norris, J. R., Eds.; Academic Press: New York, 1993; p 319.
(6) Deisenhofer, J.; Epp, O.; Miki, K.; Huber, R.; Michel, H. *J. Mol. Biol.* **1984**, *180*, 385.
(7) Michel, H.; Deisenhofer, J. *Biochemistry* **1988**, *27*, 1.
(8) Gounaris, K.; Chapman, D. J.; Booth, P. J.; et al. *FEBS Lett.* **1990**, *265*, 88.
(9) Barber, J. *Biochem. Soc. Trans.* **1993**, *21*. 981.
(10) Holzwarth, A. R. *Quart. Rev. Biophys.* **1989**, *22*, 239.
(11) van Kan, P. J. M.; Otte, S. C. M.; Kleinherenbrink, F. A. M.; Nieveen, M. C.; Aartsma, T. J.; van Gorkman, H. J. *Biochim. Biophys. Acta* **1990**, *1020*, 146.
(12) Tetenkin, V. L.; Gulyaev, B. A.; Seibert, M.; Rubin, A. B. *FEBS Lett.* **1989**, *250*, 459.
(13) Kwa, S. L. S.; Tilly, N. T.; Eijckelhoff, C.; van Grondelle, R.; Dekker, J. P. *J. Phys. Chem.* **1994**, *98*, 7712.
(14) Roelofs, T. A.; Gilbert, M.; Shuvalov, V. A.; Holzwarth, A. R. *Biochim. Biophys. Acta* **1991**, *1060*, 237.
(15) Wasielewski, M. R.; Johnson, D. G.; Seibert, M.; Govindjee *Proc. Natl. Acad. Sci. U.S.A.* **1989**, *86*, 524.
(16) Durrant, J. R.; Hastings, G.; Hong, Q.; Barber, J.; Porter, G.; Klug, D. R. *Chem. Phys. Lett.* **1992**, *188*, 54.
(17) Holzwarth, A. R.; Müller, M. G.; Gatzen, G.; Hucke, M.; Griebenow, K. *J. Lumin.* **1994**, *60,61*, 497.
(18) Gatzen, G.; Müller, M. G.; Griebenow, K.; Holzwarth, A. R. *J. Phys. Chem.* **1996**, *100*, 7269−7278.
(19) Durrant, J. R.; Hastings, G.; Joseph, D. M.; Barber, J.; Porter, G.; Klug, D. R. *Biochemistry* **1993**, *32*, 8259.
(20) Wiederrecht, G. P.; Seibert, M.; Govindjee; Wasielewski, M. R. *Proc. Natl. Acad. Sci. U.S.A.* **1994**, *91*, 8999.
(21) Müller, M. G.; Hucke, M.; Reus, M.; Holzwarth, A. R. *J. Phys. Chem.* **1996**, *100*, 9527.
(22) Bixon, M.; Jortner, J.; Michel-Beyerle, M. E. *Chem. Phys.* **1995**, *197*, 389.
(23) Ogrodnik, A.; Keupp, W.; Volk, M.; Aumeier, G.; Michel-Beyerle, M. E. *J. Phys. Chem.* **1994**, *98*, 3432.
(24) Groot, M. L.; Peterman, E. J.; van Kan, P. J. M.; van Stokkum, I. H. M.; Dekker, J. P.; van Grondelle, R. *Biophys. J.* **1994**, *67*, 318.
(25) Peloquin, J. M.; Williams, J. C.; Lin, X.; et et. *Biochemistry* **1994**, *33*, 8089.
(26) Müller, M. G.; Dorra, D.; Holzwarth, A. R.; Gad'on, N.; Drews, G. In *Photosynthesis: from Light to Biopshere*; Mathis, P., Ed.; Kluwer Academic Publishers: Dordrecht, 1995; p 595; Vol. I.
(27) Holzwarth, A. R.; Müller, M. G. *Biochemistry* 1996. In press.
(28) Konermann, L.; Holzwarth, A. R. *Biochemistry* **1996**, *35*, 829.
(29) Rebane, K. K. *Impurity Spectra of Solids. Elementary Theory of Vibrational Structure*; Plenum Press: New York, 1970.
(30) Pullerits, T.; van Mourik, F.; Monshouwer, R.; Visschers, R. W.; van Grondelle, R. *J. Lumin.* **1994**, *58*, 168.
(31) Tang, D.; Jankowiak, R.; Seibert, M.; Yocum, C. F.; Small, G. J. *J. Phys. Chem.* **1990**, *94*, 6519.
(32) Chang, H.-C.; Small, G. J.; Jankowiak, R. *Chem. Phys.* **1995**, *194*, 323.
(33) Chang, H.-C.; Jankowiak, R.; Reddy, N. R. S.; et al. *J. Phys. Chem.* **1994**, *98*, 7717.
(34) Jankowiak, R.; Tang, D.; Small, G. J.; Seibert, M. *J. Phys. Chem.* **1989**, *93*, 1649.
(35) Konermann, L.; Yruela, I.; Holzwarth, A. R. *Biochemistry* 1997. In press.
(36) Kwa, S. L. S.; Eijckelhoff, C.; van Grondelle, R.; Dekker, J. P. *J. Phys. Chem.* **1994**, *98*, 7702.
(37) Ruffle, S. V.; Donnelly, D.; Blundell, T. L.; Nugent, J. H. *Photosynth. Res.* **1992**, *34*, 287.
(38) van Leeuwen, P. J.; Nieveen, M. C.; van de Meent, E. J.; Dekker, J. P.; van Gorkom, H. J. *Photosynth. Res.* **1991**, *28*, 149.
(39) Beauregard, M.; Martin, I.; Holzwarth, A. R. *Biochim. Biophys. Acta* **1991**, *1060*, 271.
(40) Pullerits, T.; Freiberg, A. *Biophys. J.* **1992**, *63*, 879.
(41) Forster, T. In *Modern Quantum Chemistry*, Part III (Action of Light and Organic Crystals); Sinanoglu, O., Ed.; Academic Press: New York, 1965; p 93.
(42) Shipman, L. L., Housman, D. L. *Photochem. Photobiol.* **1979**, *29*, 1163.
(43) Knox, R. S.; Gülen, D. *Photochem. Photobiol.* **1993**, *57*, 40.
(44) Jean, J. M.; Fleming, G. R.; Chan, C.-K. *Isr. J. Chem.* **1988**, *28*, 169.
(45) Trinkunas, G.; Holzwarth, A. R. *Biophys. J.* **1994**, *66*, 415.
(46) Holzwarth, A. R. In *Biophysical Techniques. Advances in Photosynthesis Research*; Amesz, J., Hoff, A., Eds.; Kluwer Academic: Boston, 1996.
(47) Beechem, J. M.; Ameloot, M.; Brand, L. *Anal. Instrum.* **1985**, *14*, 379.
(48) Jankowiak, R.; Hayes, J. M.; Small, G. J. *Chem. Rev.* **1993**, *93*, 1471.
(49) Eads, D. D.; Webb, S. P.; Owens, T. G.; Mets, L.; Alberte, R. S.; Fleming, G. R. In *Progress Photosynthesis Research 1*; Biggins, J., Ed.; Nijhoff: Dordrecht, 1987; p 135.
(50) Ide, J. P.; Klug, D. R.; Dühlbrandt, W.; Giorgi, L. B.; Porter, G. *Biochim. Biophys. Acta* **1987**, *893*, 349.
(51) Roelofs, T. A.; Lee, C.-H.; Holzwarth, A. R. *Biophys. J.* **1992**, *61*, 1147.
(52) Seely, G. R.; Connolly, J. S. In *Light Emission by Plants and Bacteria*; Govindjee, Amesz, J., Fork, D. C., Eds.; Academic Press: New York, 1986; p 99.
(53) Strickler, S. J.; Berg, R. A. *J. Chem. Phys.* **1962**, *37*, 814.
(54) Sauer, K.; Scheer, H. *Biochim. Biophys. Acta* **1988**, *936*, 157.
(55) Deisenhofer, J.; Epp, O.; Miki, K.; Huber, R.; Michel, H. *Nature* **1985**, *318*, 618.
(56) Marcus, R. A.; Sutin, N. *Biochim. Biophys. Acta* **1985**, *811*, 265.
(57) Moser, C. C.; Keske, J. M.; Warncke, K.; Farid, R. S.; Dutton, P. L. *Nature* **1992**, *355*, 796.
(58) Holland, J. H. *Spektrum der Wissenschaft* **1992**, *9*, 44.
(59) Goldberg, D. E. *Genetic Algorithms in Search, Optimization, and Machine Learning*; Addison-Wesley: New York; 1989.
(60) Roelofs, T. A.; Kwa, S. L. S.; van Grondelle, R.; Dekker, J. P.; Holzwarth, A. R. *Biochim. Biophys. Acta* **1993**, *1143*, 147.
(61) Pullerits, T.; Freiberg, A. *Chem. Phys.* **1991**, *149*, 409.
(62) Pullerits, T.; Visscher, K. J.; Hess, S.; et al. *Biophys. J.* **1994**, *66*, 236.
(63) Hess, S.; Akesson, E.; Cogdell, R. J.; Pullerits, T.; Sundström, V. *Biophys. J.* **1995**, *69*, 2211.
(64) Sharkov, A. V.; Kryukov, I. V.; Khoroshilov, E. V.; et al. *Chem. Phys. Lett.* **1992**, *191*, 633.
(65) Durrant, J. R.; Hastings, G.; Joseph, D. M.; Barber, J.; Porter, G.; Klug, D. R. *Proc. Natl. Acad. Sci. U.S.A.* **1992**, *89*, 11632.
(66) Johnson, S. G.; Lee, I.-J.; Small, G. J. In *Chlorophylls*; Scheer, H., Ed.; CRC Press: Boca Raton, 1991; p 739.
(67) Reddy, N. R. S.; Lyle, P. A.; Small, G. J. *Photosynth. Res.* **1992**, *31*, 167.
(68) Schelvis, J. P. M.; van Noort, P. I.; Aartsma, T. J.; van Gorkom, H. J. In *Research in Photosynthesis*; Murata, N., Ed.; Kluwer Academic Publishers: Dordrecht, 1992; p 81; Vol. II.
(69) Vacha, F.; Joseph, D. M.; Durrant, J. R.; et al. *Proc. Natl. Acad. Sci. U.S.A.* **1995**, *92*, 2929.
(70) Schelvis, J. P. M.; van Noort, P. I.; Aartsma, T. J.; van Gorkom, H. J. *Biochim. Biophys. Acta* **1994**, *1184*, 242.
(71) Booth, P. J.; Crystall, B.; Giorgi, L. B.; Barber, J.; Klug, D. R.; Porter, G. *Biochim. Biophys. Acta* **1990**, *1016*, 141.
(72) Arlt, T.; Schmidt, S.; Kaiser, W.; et al. *Proc. Natl. Acad. Sci. U.S.A.* **1993**, *90*, 11757.
(73) Visser, H. M.; Groot, M.-L.; van Mourik, F.; van Stokkum, I. H. M.; Dekker, J. P.; van Grondelle, R. *J. Phys. Chem.* **1995**, *99*, 15304.